

Theory of active self-organization of dense nematic structures in actin gels

Waleed Mirza^{1,2}, Marco De Corato³, Marco Pensalfini¹, Guillermo

Vilanova¹, Alejandro Torres-Sánchez^{1,4,5*}, Marino Arroyo^{1,4,6*}

¹*LaCàN, Universitat Politècnica de Catalunya BarcelonaTech, 08034 Barcelona, Spain*

²*Barcelona Graduate School of Mathematics (BGSMath), 08193 Bellaterra, Spain*

³*Aragon Institute of Engineering Research (I3A), University of Zaragoza, Zaragoza, Spain*

⁴*Institute for Bioengineering of Catalonia (IBEC),*

The Barcelona Institute of Science and Technology (BIST), 08028 Barcelona Spain

⁵*European Molecular Biology Laboratory, 08003 Barcelona, Spain*

⁶*Centre Internacional de Mètodes Numèrics en Enginyeria (CIMNE), 08034 Barcelona, Spain*

(Dated: June 28, 2023)

The actin cytoskeleton is remarkably adaptable and multifunctional. It often organizes into nematic bundles such as contractile rings or stress fibers. However, how a uniform and isotropic actin gel self-organizes into dense nematic bundles is not understood. Here, using an active gel model accounting for nematic order and density variations, we identify a novel active patterning mechanism leading to dense nematic structures. Linear stability analysis and nonlinear finite element simulations establish the conditions for nematic bundle self-assembly and how active gel parameters control the architecture, orientation, connectivity and dynamics of self-organized patterns. Finally, we substantiate with discrete network simulations the main requirements for nematic bundle formation according to our theory, namely increased active tension perpendicular to the nematic direction and generalized active forces conjugate to nematic order. Our work portrays actin gels a reconfigurable active materials with a spontaneous tendency to develop patterns of dense nematic bundles.

INTRODUCTION

Actin networks are remarkably dynamic and versatile and organize in a variety of architectures to accomplish crucial cellular functions [1]. For instance, isotropic thin actin gels form the cell cortex, which largely determines cell shape [2] and motility in confined non-adherent environments [3, 4]. Polar structures at the edge of adherent cells, either forming filaments as in filopodia or sheets as in lamellipodia [5], enable cells to probe their environment and crawl on substrates. Nematic actin bundles conform a variety of contractile structures [6], including sub-cellular rings during cytokinesis [7] and cortical repair [8], supra-cellular rings during wound healing [9] or development [10], bundle networks during cellularization [11], or stress fibers in adherent cells [12–14]. Nematic bundles consist of highly aligned and densely packed actin filaments of mixed polarity connected by a diversity of crosslinkers. In vivo and in vitro observations show the key role of actin nucleators and regulators, of myosin activity and of crosslinkers in the assembly and maintenance of actin bundles [1, 2, 5, 6, 13, 15–21].

Various studies have emphasized the morphological, dynamical, molecular and functional specificities of different types of actin bundles such as dorsal, transverse, and ventral stress fibers or contractile rings [13, 14, 22–24]. Here, we ask the question of whether, despite this diversity, the ubiquity of actin bundles in different contexts can be explained by the intrinsic ability of the active actomyosin gel to self-organize into patterns of dense nematic structures. Suggestive of such active self-organization, stress fibers often form dynamic highly organized patterns, e.g. involving families of fibers along orthogonal directions [12, 14, 19, 22, 25–27]. Other kinds of actin bun-

dles also develop patterns of remarkable regularity. For instance, parallel arrangements of 2 μm -spaced actin bundles serve as templates for extra-cellular matrix deposition during butterfly wing morphogenesis and determine their iridescence [28]. Similarly, the morphogenesis of the striated tracheal cuticle in *Drosophila* is pre-patterned by a parallel arrangement of actin bundles spaced by $\sim 1 \mu\text{m}$, spanning from sub-cellular to supra-cellular and organ scales [21, 29]. Muscle-like actin bundles form regular parallel patterns spanning organs as in *C. elegans* [19] or the entire organism of hydra [30]. Furthermore, dense nematic bundles have been shown to form de novo from the sparse isotropic cortex in a process controlled by myosin activity [20], and have been shown to form a mechanically integrated network with the cortex [31].

Despite this evidence, the mechanisms underlying the spontaneous self-assembly of dense actin bundles from a low-density isotropic cortex have not been identified. Here, we develop a theory for the self-organization of dense nematic structures in the actomyosin cytoskeleton based on a nematic active gel theory in the spirit of [7, 32, 33] but extended to account for density variations and compressibility [34]. In our theory, nematic patterning is driven by activity rather than by a more conventional crowding mechanism [35, 36]. Linear stability analysis and fully nonlinear simulations show that, when coupled to nematodynamics, the well-known patterning mechanism based on self-reinforcing flows [29, 37, 38] leads to a rich diversity of patterns combining density and nematic variations. The geometry and dynamics of our patterns bear striking similarity with those observed in cells. Finally, we test the key requirements on phenomenological activity parameters for such self-organization according to our theory using discrete net-

work simulations.

RESULTS

Theoretical model. We describe a thin layer actomyosin cytoskeleton with a 2D nematic active gel theory [34]. A number of active cellular and cytoskeletal systems have been modeled using nematic active liquid-crystal theory, including dense colonies of elongated cells or dense confined cytoskeletal gels [39–41]. In such systems, crowding drives strong nematic order everywhere except at defects, which are generated by activity or required by topology [36]. We argue that the porous actin cytoskeleton is not a nematic liquid-crystal because it can adopt extended isotropic/low-order phases, and hence defects are not topologically required. Furthermore, the main mechanism driving nematic order in actomyosin gels is active contractility [19, 20, 22]. Finally, liquid crystals are nearly incompressible, whereas actin gels develop large density variations. We thus consider an active gel model capable of accommodating large density variations and in which nematic ordering is actively driven.

At time t and position \mathbf{x} , the local state of the system is described by the areal density of cytoskeletal material $\rho(t, \mathbf{x})$ and by the network architecture given by the symmetric and traceless nematic tensor $\mathbf{q}(t, \mathbf{x})$, see Fig. 1a. Assuming a fixed volumetric density ρ_{vol} , ρ can be mapped to cytoskeletal thickness ρ/ρ_{vol} . The nematic tensor can be expressed as $q_{ij} = S(n_i n_j - \delta_{ij}/2)$, where \mathbf{n} is the average molecular alignment, $S = \sqrt{2q_{ij}q_{ij}}$ the degree of local alignment about \mathbf{n} and δ_{ij} is the Kronecker delta; here and in the following we use Einstein summation convention for repeated indices. We denote by $\mathbf{v}(t, \mathbf{x})$ the velocity field of the gel and by $\mathbf{d} = \frac{1}{2}(\nabla\mathbf{v} + \nabla\mathbf{v}^T)$ and $\mathbf{w} = \frac{1}{2}(\nabla\mathbf{v} - \nabla\mathbf{v}^T)$ the rate-of-deformation and spin tensors. The rate of change of \mathbf{q} relative to a frame that translates and locally rotates with the flow generated by \mathbf{v} is given by the Jaumann derivative $\hat{\mathbf{q}} = \partial\mathbf{q}/\partial t + \mathbf{v} \cdot \nabla\mathbf{q} - \mathbf{w} \cdot \mathbf{q} + \mathbf{q} \cdot \mathbf{w}$ [42].

Based on Onsager’s variational formalism for irreversible thermodynamics [43, 44], we systematically derive the governing equations summarized next and as detailed in [34]. Because we consider a bi-periodic domain, we ignore other boundary conditions. Transport and turnover of the cortical material is described by

$$\frac{\partial\rho}{\partial t} + \nabla \cdot (\rho\mathbf{v}) - D\Delta\rho + k_d(\rho - \rho_0) = 0, \quad (1)$$

where D is an effective diffusivity, ρ_0 is the steady-state areal density and k_d is the depolymerization rate. Balance of linear momentum takes the form $\rho\gamma\mathbf{v} = \nabla \cdot \boldsymbol{\sigma}$, where $\gamma > 0$ models friction with a background medium and $\boldsymbol{\sigma}$ is the Cauchy stress tensor, which in 2D has units

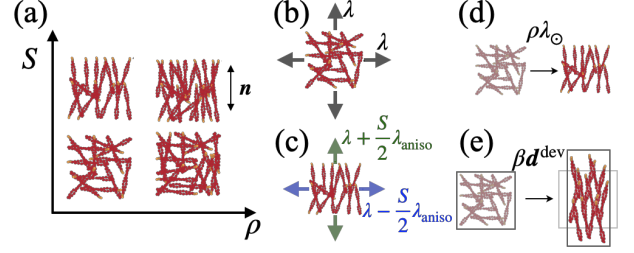


FIG. 1. **Key model ingredients.** (a) The local state is defined by areal density ρ and by orientational order quantified by the nematic parameter S and by the nematic direction \mathbf{n} . (b) Isotropic active tension λ when the network is isotropic ($S = 0$), and (c) anisotropic tension when $S \neq 0$, controlled by $\kappa = \lambda_{\text{aniso}}/\lambda$. Orientational order is driven by (d) active forces conjugate S and characterized by parameter λ_{\odot} and by (e) passive flow-induced alignment in the presence of deviatoric rate-of-deformation with coupling parameter β .

of tension. This tensor is not symmetric and reads

$$\sigma_{ij} = \rho \left\{ 2\eta(d_{ij} + d_{kk}\delta_{ij}) + \beta\hat{q}_{ij} + \sigma_{ij}^{\text{act}} - L \left[\nabla_i q_{kl} \nabla_j q_{kl} - \frac{1}{\rho} q_{ik} \nabla_l (\rho \nabla_l q_{jk}) + \frac{1}{\rho} q_{jk} \nabla_l (\rho \nabla_l q_{ik}) \right] \right\}, \quad (2)$$

where $\eta > 0$ is the shear viscosity, $\beta < 0$ measures the dissipative coupling between nematic order and strain rate [7], which here induces a stress proportional to changes in nematic tensor, σ_{ij}^{act} is the active tension resulting from mechanical transduction of chemical power in the gel, and $L > 0$ is the Frank constant. To model the dependence of contractility on network architecture, we assume

$$\sigma_{ij}^{\text{act}} = \lambda\delta_{ij} + \lambda_{\text{aniso}}q_{ij} = \lambda(\delta_{ij} + \kappa q_{ij}), \quad (3)$$

where $\kappa = \lambda_{\text{aniso}}/\lambda$ measures the sign and strength of active tension anisotropy. When order is low ($S \approx 0$), active tension is isotropic, Fig. 1b, whereas when order is high, active tension becomes anisotropic, Fig. 1c, with active tension along the nematic direction reflecting the sliding of antiparallel fibers driven by myosin motors, and perpendicular to it reflecting the out-of-equilibrium binding of bundling proteins or myosins [5, 45–51].

Balance of the generalized forces power-conjugate to $\hat{\mathbf{q}}$ also includes viscous, elastic-nematic and active contributions, and takes the form

$$\eta_{\text{rot}}\hat{\mathbf{q}} + \beta\mathbf{d}^{\text{dev}} + (2a + bS^2)\mathbf{q} - L \left(\Delta\mathbf{q} + \nabla\mathbf{q} \cdot \frac{\nabla\rho}{\rho} \right) - \rho\lambda_{\odot}\mathbf{q} = \mathbf{0}, \quad (4)$$

where η_{rot} is a nematic viscous coefficient, the second term models alignment induced by strain rate (Fig. 1e) with the deviatoric part of the rate-of-deformation tensor given by $d_{ij}^{\text{dev}} = d_{ij} - (d_{kk}/2)\delta_{ij}$, and $a > 0$ and $b > 0$ are

susceptibility coefficients. The last term is an active generalized force controlled by activity parameter $\lambda_{\odot} \geq 0$ tending to further align filaments (Fig. 1d) [7]. This term is linear in ρ because in the expansion $\lambda_{\odot} + \rho\lambda_{\odot}$ the constant contribution $\bar{\lambda}_{\odot}$ can be subsumed by the susceptibility parameter a . Thus, the active term acts as a negative density-dependent susceptibility. When $c_0 = 2a - \rho_0\lambda_{\odot} < 0$, the system can sustain a uniform quiescent state with $\rho(\mathbf{x}, t) = \rho_0$, $\mathbf{v}(\mathbf{x}, t) = 0$ and a non-zero nematic tensor satisfying $S^2 = -c_0/b$. Even if $c_0 > 0$ and hence the uniform quiescent state is devoid of order, pattern formation can induce density variations such that $2a - \rho\lambda_{\odot}$ becomes locally negative and actively favors local nematic order. The entropy production inequality requires that $2\eta\eta_{\text{rot}} - \beta^2 \geq 0$ [34].

By freezing an isotropic state, $S = 0$, our model reduces to an orientation-independent active gel model, which develops periodic patterns driven by self-reinforcing active flows sustained by diffusion and turnover [29]. In the present model, however, translational, orientational and density dynamics are intimately coupled through the terms involving β , λ_{\odot} , κ and L .

We readily identify the hydrodynamic length $\ell_s = \sqrt{\eta/\gamma}$, above which friction dominates over viscosity, the Damköhler length $\ell_D = \sqrt{D/k_d}$ above which reactions dominate over diffusion, and the nematic length $\ell_q = \sqrt{L/|2a - \lambda_{\odot}\rho_0|}$. Non-dimensional analysis reveals a set of non-dimensional groups that control the system behavior, namely the non-dimensional turnover rate $\bar{k}_d = \ell_s^2/\ell_D^2$, the Frank constant $\bar{L} = L/(\eta D)$, the susceptibility parameters $\bar{a} = a/(\gamma D)$ and $\bar{b} = b/(\gamma D)$, the drag coefficients $\bar{\eta}_{\text{rot}} = \eta_{\text{rot}}/\eta$ and $\bar{\beta} = \beta/\eta$, the nematic activity coefficient $\bar{\lambda}_{\odot} = \rho_0\lambda_{\odot}/(\gamma D)$, and the active tension parameters $\bar{\lambda} = \lambda/(\gamma D)$ and κ . The full list of material parameters for each figure given in Supplementary Tables (I,II) and justified in [52].

Onset and nature of pattern formation. To examine the role of nematic order in the emergence of various actin architectures, we performed linear stability analysis of our model particularized to 1D, whose dynamical variables are velocity, density and nematic order, $v(x, t)$, $\rho(x, t)$, and $q(x, t)$, along x , where $q > 0$ (< 0) corresponds to a nematic orientation \mathbf{n} parallel (perpendicular) to the x -axis [52]. We first focused on the case $c_0 = 2a - \rho_0\lambda_{\odot} > 0$ to examine the loss of stability of a uniform, isotropic, and quiescent steady state ($\rho(x, t) = \rho_0$, $v(x, t) = 0$, $q(x, t) = 0$) by increasing the master activity parameter λ and identifying the most unstable modes. This allowed us to determine a threshold activity for pattern formation and the wavelength of the emerging pattern. Since the exact evaluation of such quantities requires solving nonlinear equations, we derived explicit expansions in the limit of small L for the critical contractile activity

$$\lambda_{\text{crit}} \approx \lambda_{\text{crit},0} \left[1 - \frac{1}{2} \frac{\ell_s}{\ell_D} \left(1 + 2 \frac{\ell_s}{\ell_D} \right) \delta \right] + \mathcal{O}(\delta^2), \quad (5)$$

where $\lambda_{\text{crit},0} = (\sqrt{\gamma D} + 2\sqrt{k_d\eta})^2 = \gamma D(1 + 2\sqrt{\ell_s/\ell_D})^2$ and $\delta = \gamma D\kappa\beta/(2\eta c_0)$, and for the the corresponding wavenumber

$$\nu_{\text{crit}}^2 \approx \nu_{\text{crit},0}^2 \left[1 + \frac{1}{8} \left(1 + 2 \frac{\ell_s}{\ell_D} \right)^2 \delta \right] + \mathcal{O}(\delta^2), \quad (6)$$

where $\nu_{\text{crit},0}^2 = [k_d\gamma/(4\eta D)]^{1/2} = 1/(2\ell_s\ell_D)$.

The active origin of pattern formation in our model is evident from these expressions. When $\kappa = 0$ or $\beta = 0$, and hence $\delta = 0$, we recover the predictions of an active gel model not accounting for network architecture [29], $\lambda_{\text{crit}} = \lambda_{\text{crit},0}$ and $\nu_{\text{crit}} = \nu_{\text{crit},0}$. However, active tension anisotropy ($\kappa \neq 0$) and flow-induced alignment ($\beta < 0$) fundamentally change the nature of pattern formation. Nematic order introduces quantitative changes in critical tension and wavenumber, which can be very significant depending on the ratio of hydrodynamic and Damköhler lengths and on the strength and sign of nematic coupling. The nematic corrections increase as $c_0 \rightarrow 0$, close to the point where the uniform quiescent state develops spontaneous order. We thus studied separately the regime $0 < c_0 \ll 1$ [52], finding analogous expansions for the critical tension and wavenumber in terms of $\delta = \gamma D\kappa\beta/(2\eta L)$. Interestingly, Eq. (5) shows that the activity threshold is reduced, and hence pattern formation facilitated, when $\kappa < 0$, i.e. when active tension is larger perpendicular to the nematic direction. Besides modifying critical tension and wavenumber, the present model predicts that the dynamical modes with self-reinforcing flows generate patterns where high density co-localizes with high nematic order.

To test the validity of this analysis and further understand the system beyond the onset of pattern formation, we performed fully non-linear finite element simulations in a periodic 2D domain [34]. In these simulations, we increased the activity parameter λ beyond the instability starting from a quiescent uniform state. We found that the linear stability analysis very accurately predicts the activity thresholds and pattern wave-numbers within two percent across a wide range of parameters. In the nonlinear regime, the exponentially-growing instabilities eventually reach out-of-equilibrium quasi-steady-state patterns involving self-reinforcing flows towards regularly-spaced regions of high density surrounded by a low density matrix. In the absence of nematic coupling ($\beta = \kappa = \lambda_{\odot} = 0$), these high density domains are droplets arranged in a regular hexagonal lattice with $S = 0$ throughout the domain, Movie 1 [52]. In contrast, for a generic parameter set with finite β , κ and λ_{\odot} , high density domains adopt elongated configurations or bands where order is high, surrounded by a low density and low order matrix, Fig. 2b and Movie 2 [52]. Thus, the shape and internal architecture of dense phases are qualitatively modified by the nematic coupling.

Our simulations show that self-reinforcing flows develop along the direction of largest active tension, and consequently the pattern architecture depends on the

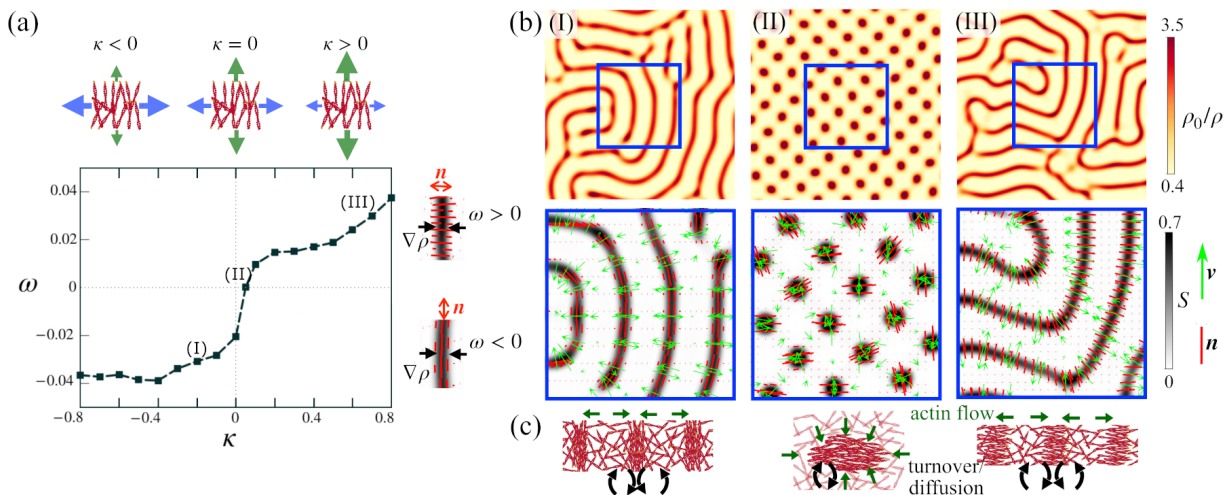


FIG. 2. **Active patterns coupling nematic order and density driven by self-reinforcing flows.** (a) Dimensionless order parameter characterizing relative orientation of nematic direction and high-density bands given by $\omega = \ell_s^2 / (\rho_0^2 |A|) \int_A \nabla \rho \cdot \mathbf{q} \nabla \rho \, dS$ as a function of active tension anisotropy parameter κ , showing transition from states with nematic direction parallel to high-density structures ($\omega < 0$, fibrillar patterns) for $\kappa < 0$ to states with nematic direction perpendicular to high-density structures ($\omega > 0$, sarcomeric patterns) for $\kappa > 0$. (b) Map of density, nematic order S , nematic direction (red segments) and flow field (green arrows) for quasi-steady fibrillar (I) and sarcomeric (III) patterns, and for a transition pattern of high density droplets with high nematic order (II) corresponding to nearly isotropic active tension. (c) These quasi-steady states are out-of-equilibrium and maintained by self-reinforcing flows, diffusion and turnover.

sign of κ , Fig. 2c. For $\kappa < 0$, the system self-organizes into high-density and high-order bands, where nematic direction is parallel to their axis, in what we call *fibrillar pattern*, Fig. 2b(I). Instead, for $\kappa > 0$ nematic order is perpendicular to the axis of the bands, in what we call *sarcomeric pattern*, Fig. 2b(III). To systematically study the effect of active tension anisotropy, we varied κ between -0.8 and 0.8 while keeping all other non-dimensional groups fixed and setting λ to be 1.3 times the critical activity. We defined the order parameter ω , Fig. 2a, allowing us to distinguish between sarcomeric ($\omega > 0$) and fibrillar ($\omega < 0$) organizations. We found a sharp transition between fibrillar and sarcomeric regimes around $\kappa \approx 0$, during which elongated high-density and high-order domains fragment into nematic droplets or tactoids, Fig. 2b(II), which have been observed in reconstituted systems [53, 54].

Our results for $\kappa < 0$, leading to self-organized dense nematic fibrillar patterns from an isotropic low-density network, are in agreement with evidence suggesting that stress fibers can assemble from the actin cortex without the involvement of stress fiber precursors or actin polymerization at focal adhesions [20], and with the spontaneous organization of reconstituted actin networks following addition of bundling agents [55]. They also agree with observations showing that actin bundles form a mechanical continuum with the surrounding sparse and isotropic cortex [31]. Their morphology and patterning dynamics is strikingly reminiscent of actin microridges, formed at the apical surfaces of mucosal epithelial cells [56, 57]. Finally, we also note the similarity in terms of density and nematic architecture between our

fibrillar patterns and those emerging in other active systems through different mechanisms of self-organization, including polar motile filaments [58, 59] or mean-field models of dry mixtures of microtubules and motors [60].

Requirements for fibrillar and sarcomeric patterns. At linear order, our theory shows that the distinctly nematic self-organization requires both flow-induced alignment (β) and active tension anisotropy (κ), whereas no condition is required on nematic activity (λ_\odot). We performed further simulations to establish the requirements for fibrillar and sarcomeric active patterning in the nonlinear regime. We found that both sarcomeric and fibrillar patterns readily form for $\beta = 0$ and finite κ , yet a finite value of β enhances fibrillar formation, leading to longer and more stable dense bands, and hinders sarcomeric organization, Movie 3 [52]. This behavior is expected since the velocity gradients of the self-reinforcing flows tend to align filaments parallel to high-density bands due to $\beta \mathbf{d}^{\text{dev}}$ in Eq. (4).

The active nematic coefficient λ_\odot modifies the onset of pattern formation through c_0 according to linear stability analysis. Apart from this linear effect, it should also contribute to condensation in high-density regions since it appears multiplied by ρ in Eq. (4). To examine this nonlinear effect, we perform simulations with $\lambda_\odot = 0$ but keeping c_0 fixed. This leads to very different patterns without clear elongated structures and very mild nematic patterning, Supplementary Figure 1(a). Enhancing nematic patterning by considering the largest thermodynamically allowed value of $|\beta|$ leads to elongated structures for $\kappa < 0$, but rather than high-order co-localizing

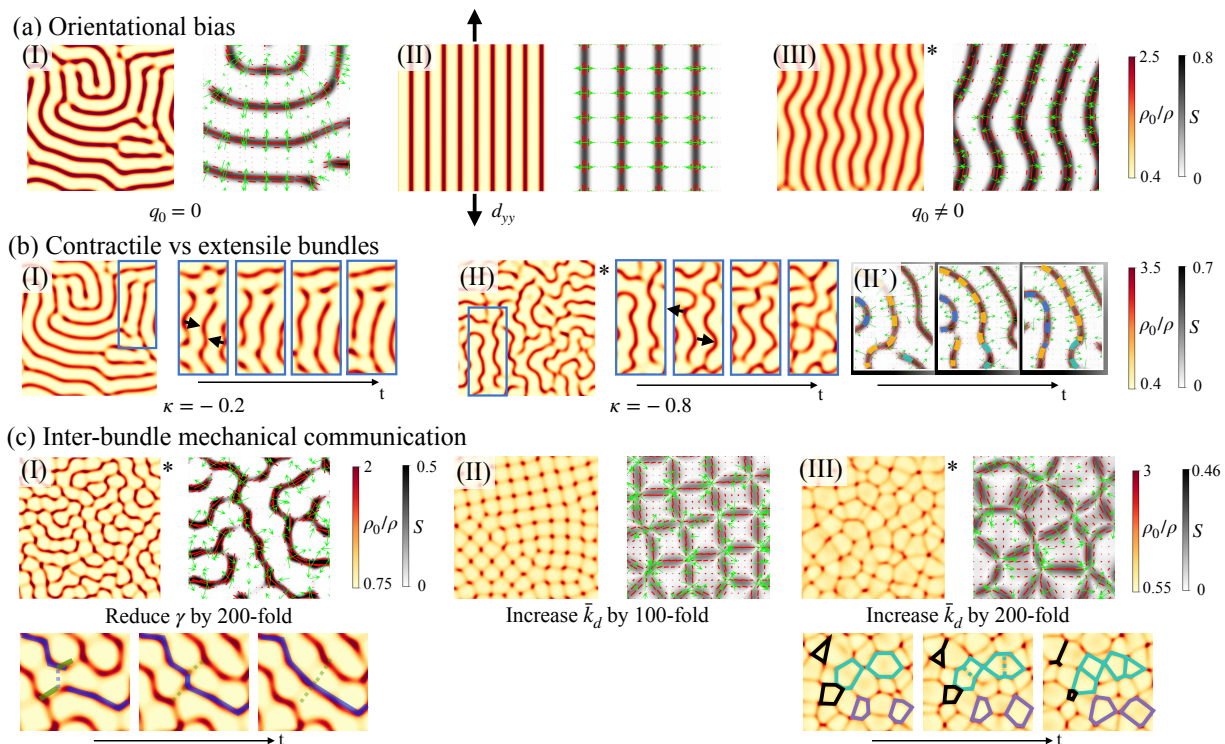


FIG. 3. **Control of nematic bundle pattern orientation, connectivity and dynamics.** (a) Effect of orientational bias. (I) A uniform isotropic gel self-organizes into a labyrinth pattern with defects. (II) A small background anisotropic strain-rate efficiently orients nematic bundles. (III) A slight initial network alignment ($S_0 = 0.05$) orients bundles, which later lose stability, bend, and generate/anneal defects. See Movie 4. (b) Depending on active tension anisotropy, nematic bundles are contractile and straighten (I, $\kappa = -0.2$), leading to quasi-steady networks, or extensile and wrinkle (II, $\kappa = -0.8$), leading to bundle breaking and recombination, and persistently dynamic networks (III). See Movie 5. (c) Promoting mechanical interaction between bundles. (I) Dynamical pattern obtained by reducing friction, and thereby increasing \bar{a} , \bar{b} , $\bar{\lambda}_0$ and \bar{k}_d . Time sequence in bottom indicates a typical reconfiguration event during which weak bundles (dashed) become strong ones (solid) and vice-versa. (II) Nearly static pattern obtained increasing \bar{k}_d , (III) which becomes highly dynamic by further increasing \bar{k}_d . Time sequence in bottom indicates the collapse (black), expansion (purple) and splitting (green) of cells in the network. See Movie 6. We indicate by * dynamical patterns exhibiting spatiotemporal chaos.

with high density, the nematic field develops domains with 90° angles between high- and low-density regions, Supplementary Figure 1(b), in an architecture enhanced by higher friction γ , Supplementary Figure 1(c). Thus, the architectures found for $\lambda_\odot = 0$ and $\kappa < 0$ are distinct from the fibrillar pattern described previously. Similarly, rather than sarcomeres, for $\lambda_\odot = 0$, $\kappa > 0$ and high $|\beta|$ we found patterns of nematic asters (high-density droplets with radial nematic organization around them), Supplementary Figure 1(b,c).

Together, these results show that active tension anisotropy ($\kappa \neq 0$) and nematic activity ($\lambda_\odot \neq 0$) are necessary and sufficient for nematic self-organization into fibrillar or sarcomeric patterns, with flow-induced alignment ($\beta < 0$) favoring fibrillar organization.

Morphological and dynamical diversity of self-organized fibrillar patterns. Given the morphological and dynamical diversity of nematic bundles in actin gels across cell types, geometric confinement, mechanical environment, or biological and pharmacological treatments

[11, 26, 27, 61–63], we varied model parameters to examine the architectures predicted by our active gel model, focusing on $\kappa < 0$. Significant changes in the effective parameters of our active gel model are reasonable since the active mechanical properties of actomyosin gels strongly depend on micro-architecture both in reconstituted systems and in cells [50, 64].

With our default parameter set, bundle junctions and free ends are unfavorable and reorganize during pattern formation to annihilate as much as possible, Movie 4(I) [52]. However, because the initial state of the system is isotropic but fibrillar patterns are not, this coarsening process leads to frustrated labyrinth patterns with domains and defects, which depending on parameters can remain frozen in quasi-steady states as in Fig. 3a(I). We then asked the questions of whether an orientational bias, which physically may be caused by cytoskeletal flows, boundaries or directed polymerization [22], could direct the pattern and result in fewer defects. We first slightly modified the system by including a small anisotropic strain-rate, according to which friction is computed rel-

ative to an elongating background. This directional bias is sufficient to produce well-oriented defect-free patterns aligned with the direction of elongation, Fig. 3a(II) and Movie 4(II) [52]. Alternatively, we considered c_0 to be slightly negative, leading to the uniform and nematic steady state $\rho(x,t) = \rho_0$, $v(x,t) = 0$ and $q(x,t) = q_0 = \pm \frac{1}{2} \sqrt{-c_0/b}$. The linear stability analysis around this state and further nonlinear simulations show that the essential phenomenology of Eqs. (5,6) and Fig. 2 is not altered by the slight pre-existing order [52]. Again, the weak pre-existing order provides sufficient bias to direct pattern orientation, Fig. 3a(III). Thus, our model indicates that an anisotropic bias can guide and anneal nematic fibrillar patterns, in agreement with remarkably oriented patterns of actin bundles in elongated cells [28], as a result of uniaxial cellular stretch [19, 57], or on anisotropically curved surfaces [21, 29].

At longer times, the nematic bundles in Fig. 3a(III) develop secondary active instabilities leading to coordinated bending, curvature amplification, defect nucleation and annihilation, Movie 4(III) [52], in a behavior reminiscent of active extensile systems. This possibility is puzzling because our active gel is contractile. To systematically examine it, we performed simulations at higher active tension anisotropies $\kappa = -0.8$, which we compared with our reference $\kappa = -0.2$, Fig. 3b. While in our reference system bundles behave like contractile objects tending to straighten, for $\kappa = -0.8$ they behave like extensile objects enhancing curvature, which results in continuous defect nucleation as highly bent bundles destabilize and fragment, as well as defect annihilation as pairs of free ends merge to reorganize the network, in a behavior akin to active turbulence [65]. See Movie 5 [52] for an illustration and for the slightly extensile case $\kappa = -0.5$. To understand the origin of this behavior, we examined the individual components of the total tension, Eq. (2), along and perpendicular to the fibrillar pattern, Supplementary Fig. 2. Because in all of these simulations active contraction is larger perpendicular to nematic bundles ($\kappa < 0$) as required for their self-assembly, bundles are effectively extensile with regards to the active component of the total tension. Competing with active tension, however, viscous tension is negative and larger perpendicular to the bundles. Hence, depending on their relative magnitude, the total tension can be larger along or perpendicular to the bundles. We found that for contractile bundles leading to stable fibrillar patterns ($\kappa = -0.2$), total tension is larger along bundles, indicating that a large fraction of the active power perpendicular to the bundles is dissipated in the self-reinforcing flows, and hence is not available to perform power at a mesoscale. Instead, for stronger active anisotropy ($\kappa = -0.8$), total tension along nematic bundles is smaller than perpendicular to them, Supplementary Fig. 2(c), confirming the extensile nature of the self-organized bundles leading to the secondary wrinkling instability. In summary, our theory predicts that a contractile nematic active gel can self-organize into fibrillar patterns with mesoscale bundles that are either contrac-

tile or extensile depending on the parameter regime.

Focusing on contractile bundles, we then examined a different parameter regime known to trigger sustained pattern dynamics. For isotropic gels, previous work has shown that reducing friction triggers chaotic dynamics as the distance between high-density regions, $2\pi/\nu_{\text{crit}}$, becomes comparable or smaller than the hydrodynamic length scale [29], thus enabling their mechanical interaction. In a model devoid of orientational order, reducing friction is equivalent to increasing \bar{k}_d . In our model, however, we can either reduce γ , which in non-dimensional terms means increasing \bar{k}_d , \bar{a} , \bar{b} and $\bar{\lambda}_\odot$ in concert, or increase \bar{k}_d while leaving all other non-dimensional parameters fixed. The first of these choices leads to dynamic and hierarchical networks with very dense and highly-aligned bundles, which coexist with perpendicular weak bundles with much lower density enrichment and ordering. These two families of bundles enclose cells of isotropic and sparse gel, Fig. 3c(I). Junctions where two or more dense bundles meet are very unfavorable and short-lived, but junctions of two dense and a weak bundle are much more stable. Because bundles are mechanically coupled, the networks actively reorganizes in events where dense bundles become weak bundles and vice-versa, inset and Movie 6(I). We note that here total tension along bundles is much larger than perpendicular to them, Supplementary Fig. 2(d), and hence the persistent dynamics are unrelated to the previously described behavior of extensile bundles.

The second choice to favor mechanical interaction of bundles, increasing \bar{k}_d only, leads to very different networks with high-density aster-like clusters interconnected by straight actin bundles. Because now $\bar{\lambda}_\odot$ is not particularly large, order is low at the core of these clusters, enabling high-valence networks where four bundles often meet at one cluster. For $\bar{k}_d = 10$, the network is stable and nearly crystalline, Fig. 3b(II), whereas for $\bar{k}_d = 20$, it becomes highly dynamical and pulsatile with frequent collapse of polygonal cells by fusion of neighboring actin clusters and their attached bundles (black polygons) and nucleation of new bundles within large low-density cells (dashed/solid green lines), Fig. 3b(III) and Movie 6(III) [52]. This architecture and dynamics resemble those of early *C. elegans* embryos [66], adherent epithelial cells treated with epidermal growth factor [27] and mouse embryonic stem cells [62]. Recent active gel models accounting for RhoA signaling develop similar pulsatile behaviors in 2D, but do not predict the orientational order of the spatio-temporal patterns of the actomyosin cortex [67].

In summary, our theory maps how effective parameters of the actin gel control the active self-organization of a uniform and isotropic gel into a pattern of high-density nematic bundles embedded in a low-density isotropic matrix, including the activity threshold, the bundle spacing, orientation, connectivity and dynamics.

Microscopic origin of $\kappa < 0$ and $\lambda_\odot > 0$ through discrete network simulations. A somewhat counter-intuitive prediction of our model is that the self-

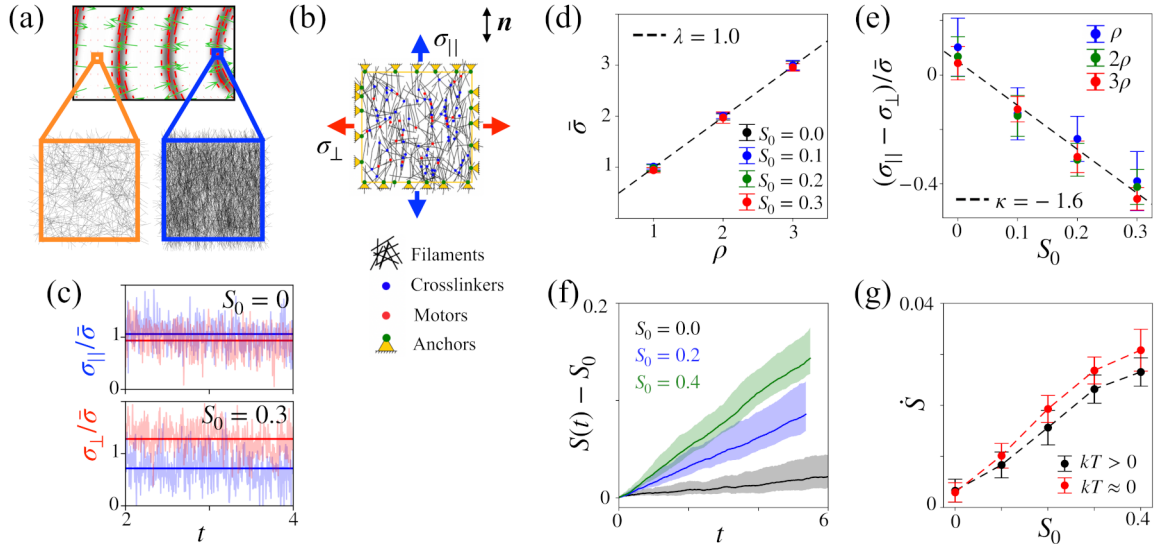


FIG. 4. **Assessment of activity parameters κ and λ_{\odot} through discrete network simulations.** (a) Illustration of the computational domain of the discrete network as a uniform representative volume element of the gel. (b) Sketch of model ingredients and setup to compute tension along and perpendicular to the nematic direction. (c) Typical time-signal for parallel and perpendicular tensions following addition of crosslinkers and motors (translucent lines) along with time average (solid lines) for isotropic and anisotropic networks. Tension is normalized by mean tension $\bar{\sigma} = (\sigma_{\parallel} + \sigma_{\perp})/2$ computed from time-averages and time by actin turnover time. (d) Mean tension as a function of network density for several nematic parameters S_0 , where both quantities are normalized by their values for the lowest density. With this normalization, Eq. (7) predicts a linear dependence with slope $\lambda = 1$ (dashed line). Error bars span two standard deviations. (e) Deviatoric tension as a function of nematic order for different densities. The dashed line is a linear regression to simulation data. (f) Dynamics of nematic order in a periodic network following addition of crosslinkers and motors for three initial values of nematic order. (g) Rate of change of nematic order normalized by turnover rate as a function of initial nematic order at zero and finite temperature.

organization of nematic bundles, the most prominent emerging organization in actin gels across cell types and length-scales, requires that active tension perpendicular to nematic orientation is larger than along this direction ($\kappa < 0$), at least at the onset of pattern formation. While our continuum hydrodynamical model can address mesoscopic conditions for self-organization, it cannot provide insight about the microscopic origin of effective activity parameters. To examine whether the conditions $\kappa < 0$ and $\lambda_{\odot} > 0$ for spontaneous formation of fibrillar patterns are plausible from a microscopic point of view, we performed discrete network simulations using Cytosim [68].

Addressing the self-organization of the actin cytoskeleton at mesoscales directly with discrete network simulations is very challenging due to the wide range in time- and length-scales and the need to realistically model diffusion, network renewal, friction and gel hydrodynamics. Instead, we aimed at characterizing the out-of-equilibrium mechanical behavior of a representative volume element of the material with uniform mesoscopic properties, Fig. 4a. We performed 2D simulations in which semi-flexible filaments interact with crosslinkers and myosin motors, all of which undergo turnover and have a stoichiometry previously used to model the actin cytoskeleton [69], Fig. 4b. See [52] for a detailed description of the simulation protocol. Briefly, we modified

Cytosim to account for average orientational order in the simulation box, which we evaluated as a sample average of orientations over the ensemble of segments composing the filaments. We further introduced a nematic energy penalty in the network allowing us to restrain average nematic order to a target value S_0 .

We first prepared a system consisting only of randomly oriented actin fibers, imposed the desired orientational order S_0 using the nematic penalty and equilibrated the system. In a first set of simulations, once S_0 was reached, we deactivated the nematic penalty and added crosslinkers and myosins, driving the system out-of-equilibrium. The free contraction of the system was prevented by the addition of anchors at the boundary of the representative volume element, which also allowed us to compute anchor forces and hence estimate the effective active tension along the nematic direction $\sigma_{\parallel} = \sigma_{ij}n_in_j$ and perpendicular to it, $\sigma_{\perp} = \sigma_{ij}m_im_j$ with $n_im_i = 0$ and $m_im_i = 1$, Fig. 4(b).

Addition of crosslinkers and myosins leads to bundling of actin filaments at the microscale, Movie 7 [52], distinct from the mesoscale fibrillar pattern formation emerging from the active gel model. It also leads to out-of-equilibrium tension as measured by the anchors. For isotropic networks ($S_0 = 0$), active tension is isotropic with $\sigma_{\parallel} \approx \sigma_{\perp}$. For anisotropic networks, however, we found that tension becomes anisotropic with $\sigma_{\perp} > \sigma_{\parallel}$,

Fig. 4(c).

We systematically characterized this behavior varying initial orientational order and network density. According to our active gel model, Eqs. (2,3), in the absence of nematic gradients and flow, the tension components σ_{\parallel} and σ_{\perp} satisfy the following relations in terms of mean and deviatoric tensions

$$\bar{\sigma} = (\sigma_{\parallel} + \sigma_{\perp})/2 = \lambda\rho \quad \text{and} \quad (\sigma_{\parallel} - \sigma_{\perp})/\bar{\sigma} = \kappa S. \quad (7)$$

Remarkably, our discrete network simulations closely followed these relations, Fig. 4(d,e), which allowed us to estimate $\kappa \approx -1.6$. We robustly found that $\kappa < 0$ for perturbations of selected parameters of the discrete network model as long as turnover rates of crosslinkers and myosins were relatively fast.

We then wondered if the discrete network simulations could provide evidence for the orientational activity parameter in our theory, $\rho\lambda_{\odot}$. For a uniform system with nematic order along a given direction and ignoring the susceptibility parameter b , Eq. (4) becomes

$$\eta_{\text{rot}}\dot{S} + (2a - \rho\lambda_{\odot})S + \mathcal{K}_S(S - S_0) = 0, \quad (8)$$

where η_{rot} is the viscous drag of the filaments in the discrete network simulations, $a > 0$ the entropic tendency of the model to return to isotropy, $\rho\lambda_{\odot}$ the active forcing of nematic order resulting from crosslinkers and motors, and the last term accounts for the effect of the nematic penalty with coefficient \mathcal{K}_S . As a first test of this model, we started from an isotropic and periodic network and tracked the athermal dynamics of S under the action of the nematic penalty in the absence of anchors, crosslinkers and myosins. For $\lambda_{\odot} = 0$ and $a = 0$, Eq. (8) predicts an exponential relaxation given by $S(t) = S_0(1 - e^{-K_S t/\eta_{\text{rot}}})$, which very closely matched the simulation data for different values of S_0 and for a single fitting parameter η_{rot} , Supplementary Fig. 3(III) and Movie 8 [52]. We then deactivated the nematic penalty and added crosslinkers and motors, but not anchors, to track unconstrained dynamics of nematic order starting from different values of S_0 . In agreement with the notion of an active force driving nematic order, we found that $S(t)$ monotonically increased, Fig. 4(f). More quantitatively, we tested the short-time prediction of Eq. (8), $\eta_{\text{rot}}\dot{S} = (\rho\lambda_{\odot} - 2a)S_0$, by plotting \dot{S} as estimated from our simulations, as a function of S_0 , Fig. 4(g). We found a nearly linear relation with positive slope, hence providing evidence for an active generalized force driving order. In agreement with the theory, in the athermal limit, the tendency to actively increase order is faster as the entropic tendency to disorder is absent ($a = 0$).

In summary, discrete network cytoskeletal simulations provide a microscopic justification for two key ingredients of our active gel theory, namely that nematic order elicits (1) anisotropic active tensions, which can be larger perpendicular to the nematic direction ($\kappa < 0$), and (2) active generalized forces driving further ordering.

CONCLUSIONS

We have developed a theory for the active self-organization of initially uniform and isotropic actin gels into various dense nematic architectures embedded in an isotropic matrix of low density. This model predicts a variety of emergent patterns involving asters, tactoids, and sarcomeric bands. More importantly, it identifies a wide parameter space where the active gel spontaneously develops patterns of dense nematic bundles, the most prominent nematic architecture across scales and cell types. We have characterized how the activity threshold, spacing, geometry, connectivity and dynamics these patterns depends on effective active gel parameters. Because these mesoscale parameters depend on the composition and dynamics of the network at the molecular scale, our results portray actin gels as responsive and reconfigurable active materials that cells can finely regulate. We have further shown that the spontaneous tendency of the gel to assemble bundle patterns can be directed via subtle cues. Thus, a combination of biochemical control of actin dynamics along with geometric, mechanical or biochemical guiding [70, 71] may explain the emergence and context-dependent organization of regular patterns of bundle networks, from sub-cellular to organism scales [12, 14, 19, 21, 22, 25–28, 30]. Consistently, perturbations of myosin contractility have been shown to alter, disorder, or even prevent the formation patterns of parallel bundles in *C. elegans* [19], whereas perturbations of actin polymerization in drosophila embryos impair the robust organization of actin bundle patterns at the cellular and organ scales by disrupting orientation and spacing, but not the tendency of the actomyosin cytoskeleton to form patterns of parallel bundles [21].

Our theory identifies two key requirements on activity parameters for the self-organization of patterns of nematic bundles, namely active tension anisotropy with larger tension perpendicular to the nematic direction and generalized active forces tending to increase nematic order. Although our discrete network simulations support these two conditions, we expect that in a different regime anisotropic tension may be larger along the nematic direction ($\kappa > 0$). For instance, once bundles are dense and maximally aligned, the ability of the active nematic gel to perform active tension perpendicular to the nematic direction may saturate, while myosin motors may contract the gel along the nematic direction more effectively. The regime studied here explains the initial assembly of dense nematic bundles, but not their maturation to become highly contractile or viscoelastic as demonstrated for stress fibers depending on different isoforms of non-muscle myosin II or on actin regulators such as zyxin [72, 73]. Our work thus suggests further experimental and computational work to establish a comprehensive mapping between molecular and mesoscale properties of the active gel, and hence a bridge between molecular regulation and emergent cytoskeletal organization.

AUTHOR CONTRIBUTIONS

WM, ATS and MA conceived the study and developed the active gel theory. WM, GV and ATS developed and implemented numerical methods. WM performed and analyzed active gel simulations. WM and MP performed and analyzed discrete network simulations. MP developed the code and simulation protocols for discrete network simulations. MDC contributed to linear stability analysis. WM and MA wrote the manuscript. ATS and MA supervised the study.

ACKNOWLEDGEMENTS

The authors acknowledge the support of the European Research Council (CoG-681434) and the Spanish Ministry for Science and Innovation (PID2019-110949GB-I00). WM acknowledges the La Caixa Fellowship and the European Union's Horizon 2020 research and innovation program under the Marie Skłodowska-Curie action (GA 713637). MP acknowledges the support from the Spanish Ministry of Science and Innovation & NextGenerationEU/PRTR (PCI2021-122049-2B). MA acknowledges the Generalitat de Catalunya (ICREA Academia prize for excellence in research). MDC acknowledges funding from the Spanish Ministry for Science and Innovation through the Juan de la Cierva Incorporación fellowship IJC2018-035270-I. IBEC and CIMNE are recipients of a Severo Ochoa Award of Excellence.

BIBLIOGRAPHY

- [1] S. Banerjee, M. L. Gardel, and U. S. Schwarz, The actin cytoskeleton as an active adaptive material, *Annual Review of Condensed Matter Physics* **11**, 421 (2020).
- [2] P. Chugh and E. K. Paluch, The actin cortex at a glance, *Journal of Cell Science* **131**, jcs186254 (2018).
- [3] H. Blaser, M. Reichman-Fried, I. Castanon, K. Dumstrei, F. L. Marlow, K. Kawakami, L. Solnica-Krezel, C.-P. Heisenberg, and E. Raz, Migration of zebrafish primordial germ cells: a role for myosin contraction and cytoplasmic flow, *Developmental Cell* **11**, 613 (2006).
- [4] V. Ruprecht, S. Wieser, A. Callan-Jones, M. Smutny, H. Morita, K. Sako, V. Barone, M. Ritsch-Marte, M. Sixt, R. Voituriez, and C.-P. Heisenberg, Cortical contractility triggers a stochastic switch to fast amoeboid cell motility, *Cell*, **Cell** **160**, 673 (2015).
- [5] L. Blanchoin, R. Boujemaa-Paterski, C. Sykes, and J. Plastino, Actin dynamics, architecture, and mechanics in cell motility, *Physiological Reviews* **94**, 235 (2014).
- [6] C. Schwayyer, M. Sikora, J. Slováková, R. Kardos, and C.-P. Heisenberg, Actin rings of power, *Developmental Cell* **37**, 493 (2016).
- [7] A.-C. Reymann, F. Staniscia, A. Erzberger, G. Salbreux, and S. W. Grill, Cortical flow aligns actin filaments to form a furrow, *eLife* **5**, e17807 (2016).
- [8] C. A. Mandato and W. M. Bement, Contraction and polymerization cooperate to assemble and close actomyosin rings around xenopus oocyte wounds, *The Journal of cell biology* **154**, 785 (2001).
- [9] P. Martin and J. Lewis, Actin cables and epidermal movement in embryonic wound healing, *Nature* **360**, 179 (1992).
- [10] M. Krieg, Y. Arboleda-Estudillo, P. H. Puech, J. Käfer, F. Graner, D. J. Müller, and C. P. Heisenberg, Tensile forces govern germ-layer organization in zebrafish, *Nature Cell Biology* **10**, 429 (2008).
- [11] O. Dudin, A. Ondracka, X. Grau-Bové, A. A. Haraldsen, A. Toyoda, H. Suga, J. Bråte, and I. Ruiz-Trillo, A unicellular relative of animals generates a layer of polarized cells by actomyosin-dependent cellularization, *eLife* **8**, e49801 (2019).
- [12] F. Senger, A. Pitaval, H. Ennomani, L. Kurzawa, L. Blanchoin, and M. Théry, Spatial integration of mechanical forces by alpha-actinin establishes actin network symmetry, *Journal of Cell Science* **132**, 10.1242/jcs.236604 (2019), jcs236604.
- [13] S. Tojkander, G. Gateva, and P. Lappalainen, Actin stress fibers—assembly, dynamics and biological roles, *Journal of Cell Science* **125**, 1855 (2012).
- [14] S. Tojkander, G. Gateva, A. Husain, R. Krishnan, and P. Lappalainen, Generation of contractile actomyosin bundles depends on mechanosensitive actin filament assembly and disassembly, *eLife* **4**, e06126 (2015).
- [15] M. Chrzanowska-Wodnicka and K. Burridge, Rho-stimulated contractility drives the formation of stress fibers and focal adhesions., *The Journal of Cell Biology* **133**, 1403 (1996).
- [16] T. Thoresen, M. Lenz, and M. L. Gardel, Reconstitution of contractile actomyosin bundles, *Biophysical Journal* **100**, 2698 (2011).
- [17] D. Strehle, S. Jorg, C. Heussinger, J. Alvarado, M. Bathe, J. Kas, and B. Gentry, Transiently crosslinked f-actin bundles, *European Biophysics Journal* **40**, 93 (2011).
- [18] D. Laporte, N. Ojkic, D. Vavylonis, and J.-Q. Wu, α -actinin and fimbrin cooperate with myosin ii to organize actomyosin bundles during contractile-ring assembly, *Molecular Biology of the Cell (MBoC)* **23**, 3094 (2012).
- [19] A. C. Wirshing and E. J. Cram, Myosin activity drives actomyosin bundle formation and organization in contractile cells of the caenorhabditis elegans spermatheca, *Molecular Biology of the Cell (MBoC)* **28**, 1937 (2017).
- [20] J. I. Lehtimäki, E. K. Rajakylä, S. Tojkander, and P. Lappalainen, Generation of stress fibers through myosin-driven reorganization of the actin cortex, *eLife* **10**, e60710 (2021).
- [21] A. Öztürk-Çolak, B. Moussian, S. J. Araújo, and J. Casanova, A feedback mechanism converts individual cell features into a supracellular ecm structure in *Drosophila* trachea, *eLife* **5**, e09373 (2016).
- [22] P. Hotulainen and P. Lappalainen, Stress fibers are generated by two distinct actin assembly mechanisms in motile cells, *The Journal of cell biology* **173**, 383 (2006).
- [23] P. Naumanen, P. Lappalainen, and P. Hotulainen, Mechanisms of actin stress fibre assembly, *Journal of Microscopy* **231**, 446 (2008).
- [24] S. Lee, E. Kassianidou, and S. Kumar, Actomyosin stress fiber subtypes have unique viscoelastic properties and roles in tension generation, *Molecular Biology of the Cell* **29**, 1992 (2018).

- [25] Y. H. Tee, T. Shemesh, V. Thiagarajan, R. F. Hariadi, K. L. Anderson, C. Page, N. Volkmann, D. Hanein, S. Sivaramakrishnan, M. M. Kozlov, *et al.*, Cellular chirality arising from the self-organization of the actin cytoskeleton, *Nature Cell Biology* **17**, 445 (2015).
- [26] L. Yolland, M. Burki, S. Marcotti, A. Luchici, F. N. Kenny, J. R. Davis, E. Serna-Morales, J. Müller, M. Sixt, A. Davidson, *et al.*, Persistent and polarized global actin flow is essential for directionality during cell migration, *Nature Cell Biology* **21**, 1370 (2019).
- [27] S. Jalal, S. Shi, V. Acharya, R. Y.-J. Huang, V. Viasnoff, A. D. Bershadsky, and Y. H. Tee, Actin cytoskeleton self-organization in single epithelial cells and fibroblasts under isotropic confinement, *Journal of Cell Science* **132**, jcs220780 (2019).
- [28] A. Dinwiddie, R. Null, M. Pizzano, L. Chuong, A. Leigh Krup, H. Ee Tan, and N. H. Patel, Dynamics of f-actin prefigure the structure of butterfly wing scales, *Developmental Biology* **392**, 404 (2014).
- [29] E. Hannezo, B. Dong, P. Recho, J.-F. Joanny, and S. Hayashi, Cortical instability drives periodic supracellular actin pattern formation in epithelial tubes, *Proceedings of the National Academy of Sciences* **112**, 8620 (2015).
- [30] Y. Maroudas-Sacks, L. Garion, L. Shani-Zerbib, A. Livshits, E. Braun, and K. Keren, Topological defects in the nematic order of actin fibres as organization centres of hydra morphogenesis, *Nature Physics* **17**, 251 (2021).
- [31] T. Vignaud, C. Copos, C. Leterrier, M. Toro-Nahuelpan, Q. Tseng, J. Mahamid, L. Blanchoin, A. Mogilner, M. Théry, and L. Kurzawa, Stress fibres are embedded in a contractile cortical network, *Nature materials* **20**, 410 (2021).
- [32] G. Salbreux, J. Prost, and J.-F. Joanny, Hydrodynamics of cellular cortical flows and the formation of contractile rings, *Physical Review Letters* **103**, 058102 (2009).
- [33] F. Jülicher, S. W. Grill, and G. Salbreux, Hydrodynamic theory of active matter, *Reports on Progress in Physics* **81**, 076601 (2018).
- [34] W. Mirza, A. Torres-Sánchez, G. Vilanova, and M. Arroyo, Variational formulation of active nematics: theory and simulation, arXiv (2023), 2306.01515 [physics.bio-ph].
- [35] M. S. e Silva, J. Alvarado, J. Nguyen, N. Georgoulia, B. M. Mulder, and G. H. Koenderink, Self-organized patterns of actin filaments in cell-sized confinement, *Soft Matter* **7**, 10631 (2011).
- [36] A. Doostmohammadi, J. Ignés-Mullol, J. M. Yeomans, and F. Sagués, Active nematics, *Nature Communications* **9**, 1 (2018).
- [37] J. S. Bois, F. Jülicher, and S. W. Grill, Pattern formation in active fluids, *Physical Review Letters* **106**, 028103 (2011).
- [38] A. Callan-Jones and R. Voituriez, Active gel model of amoeboid cell motility, *New Journal of Physics* **15**, 025022 (2013).
- [39] L. Giomi, M. J. Bowick, P. Mishra, R. Sknepnek, and M. Cristina Marchetti, Defect dynamics in active nematics, *Philosophical Transactions of the Royal Society A: Mathematical, Physical and Engineering Sciences* **372**, 20130365 (2014).
- [40] G. Duclos, C. Erlenkämper, J.-F. Joanny, and P. Silberzan, Topological defects in confined populations of spindle-shaped cells, *Nature Physics* **13**, 58 (2017).
- [41] N. Kumar, R. Zhang, J. J. de Pablo, and M. L. Gardel, Tunable structure and dynamics of active liquid crystals, *Science Advances* **4**, eaat7779 (2018).
- [42] P. de Gennes and J. Prost, *The Physics of Liquid Crystals*, International Series of Monogr (Clarendon Press, 1993).
- [43] M. Doi, Onsager’s variational principle in soft matter, *Journal of Physics: Condensed Matter* **23**, 284118 (2011).
- [44] M. Arroyo, N. Walani, A. Torres-Sánchez, and D. Kaurin, Onsager’s variational principle in soft matter: Introduction and application to the dynamics of adsorption of proteins onto fluid membranes, in *The Role of Mechanics in the Study of Lipid Bilayers*, edited by D. J. Steigmann (Springer International Publishing, Cham, 2018) pp. 287–332.
- [45] E. S. Harris, I. Rouiller, D. Hanein, and H. N. Higgs, Mechanistic differences in actin bundling activity of two mammalian formins, *Journal of Biological Chemistry* **281**, 14383 (2006).
- [46] D. S. Courson and R. S. Rock, Actin cross-link assembly and disassembly mechanics for α -actinin and fascin, *Journal of Biological Chemistry* **285**, 26350 (2010).
- [47] M. Schuppler, F. C. Keber, M. Kröger, and A. R. Bausch, Boundaries steer the contraction of active gels, *Nature Communications* **7**, 1 (2016).
- [48] J. Li, T. Biel, P. Lomada, Q. Yu, and T. Kim, Buckling-induced f-actin fragmentation modulates the contraction of active cytoskeletal networks, *Soft Matter* **13**, 3213 (2017).
- [49] S. K. Nandi, Activity-dependent self-regulation of viscous length scales in biological systems, *Physical Review E* **97**, 052404 (2018).
- [50] H. Ennomani, G. Letort, C. Guérin, J.-L. Martiel, W. Cao, F. Nédélec, E. M. D. L. Cruz, M. Théry, and L. Blanchoin, Architecture and connectivity govern actin network contractility, *Current Biology* **26**, 616 (2016).
- [51] S. Chen, T. Markovich, and F. C. MacKintosh, Motor-free contractility in active gels, *Phys. Rev. Lett.* **125**, 208101 (2020).
- [52] See supplemental material for additional information on the theoretical model, the computational algorithms and for videos illustrating the pattern formation.
- [53] K. L. Weirich, S. Banerjee, K. Dasbiswas, T. A. Witten, S. Vaikuntanathan, and M. L. Gardel, Liquid behavior of cross-linked actin bundles, *Proceedings of the National Academy of Sciences* **114**, 2131 (2017).
- [54] K. L. Weirich, K. Dasbiswas, T. A. Witten, S. Vaikuntanathan, and M. L. Gardel, Self-organizing motors divide active liquid droplets, *Proceedings of the National Academy of Sciences* **116**, 11125 (2019).
- [55] S. Deshpande and T. Pfohl, Real-time dynamics of emerging actin networks in cell-mimicking compartments, *PloS one* **10**, e0116521 (2015).
- [56] J. A. Depasquale, Actin microridges, *The Anatomical Record* **301**, 2037 (2018).
- [57] A. P. van Loon, I. S. Erofeev, I. V. Maryshev, A. B. Goryachev, and A. Sagasti, Cortical contraction drives the 3D patterning of epithelial cell surfaces, *Journal of Cell Biology* **219**, 10.1083/jcb.201904144 (2020), e201904144.
- [58] L. Huber, R. Suzuki, T. Krüger, E. Frey, and A. R. Bausch, Emergence of coexisting ordered states in active matter systems, *Science* **361**, 255 (2018).

- [59] J. Denk and E. Frey, Pattern-induced local symmetry breaking in active-matter systems., *Proc Natl Acad Sci U S A* **117**, 31623 (2020).
- [60] I. Maryshev, A. B. Goryachev, D. Marenduzzo, and A. Morozov, Dry active turbulence in a model for microtubule–motor mixtures, *Soft Matter* **15**, 6038 (2019).
- [61] M. Gupta, B. R. Sarangi, J. Deschamps, Y. Nematbakhsh, A. Callan-Jones, F. Margadant, R.-M. Mège, C. T. Lim, R. Voituriez, and B. Ladoux, Adaptive rheology and ordering of cell cytoskeleton govern matrix rigidity sensing, *Nature Communications* **6**, 1 (2015).
- [62] S. Xia, Y. B. Lim, Z. Zhang, Y. Wang, S. Zhang, C. T. Lim, E. K. Yim, and P. Kanchanawong, Nanoscale architecture of the cortical actin cytoskeleton in embryonic stem cells, *Cell Reports* **28**, 1251 (2019).
- [63] A. Verkhovskiy, T. Svitkina, and G. Borisy, Polarity sorting of actin filaments in cytochalasin-treated fibroblasts, *Journal of Cell Science* **110**, 1693 (1997).
- [64] P. Chugh, A. G. Clark, M. B. Smith, D. A. Cassani, K. Dierkes, A. Ragab, P. P. Roux, G. Charras, G. Salbreux, and E. K. Paluch, Actin cortex architecture regulates cell surface tension, *Nature cell biology* **19**, 689 (2017).
- [65] R. Alert, J. Casademunt, and J.-F. Joanny, Active turbulence, *Annual Review of Condensed Matter Physics* **13**, 143 (2022).
- [66] E. Munro, J. Nance, and J. R. Priess, Cortical flows powered by asymmetrical contraction transport par proteins to establish and maintain anterior-posterior polarity in the early *c. elegans* embryo, *Developmental Cell* **7**, 413 (2004).
- [67] M. F. Staddon, E. M. Munro, and S. Banerjee, Pulsatile contractions and pattern formation in excitable actomyosin cortex, *PLOS Computational Biology* **18**, 1 (2022).
- [68] F. Nedelec and D. Foethke, Collective langevin dynamics of flexible cytoskeletal fibers, *New Journal of Physics* **9**, 427 (2007).
- [69] D. B. Cortes, M. Gordon, F. Nédélec, and A. S. Maddox, Bond type and discretization of nonmuscle myosin ii are critical for simulated contractile dynamics, *Biophysical Journal* **118**, 2703 (2020).
- [70] P. Gross, K. V. Kumar, and S. W. Grill, How active mechanics and regulatory biochemistry combine to form patterns in development, *Annual Review of Biophysics* **46**, 337 (2017), PMID: 28532214.
- [71] T. Burkart, M. C. Wigbers, L. Würthner, and E. Frey, Control of protein-based pattern formation via guiding cues, *Nature Reviews Physics* **4**, 511 (2022).
- [72] K. Weißenbruch, J. Grewe, M. Hippler, M. Fladung, M. Tremmel, K. Stricker, U. S. Schwarz, and M. Bastmeyer, Distinct roles of nonmuscle myosin ii isoforms for establishing tension and elasticity during cell morphodynamics, *eLife* **10**, e71888 (2021).
- [73] P. W. Oakes, E. Wagner, C. A. Brand, D. Probst, M. Linke, U. S. Schwarz, M. Glotzer, and M. L. Gardel, Optogenetic control of rhoa reveals zyxin-mediated elasticity of stress fibres, *Nature Communications* **8**, 15817 (2017).